

CrossMark
click for updatesCite this: *Catal. Sci. Technol.*, 2016,
6, 7569

A low-temperature approach to synthesize low-silica SAPO-34 nanocrystals and their application in the methanol-to-olefins (MTO) reaction†

Beibei Gao,^{ab} Miao Yang,^a Yuyan Qiao,^{ab} Jinzhe Li,^a Xiao Xiang,^{ab} Pengfei Wu,^{ab}
Yingxu Wei,^a Shutao Xu,^a Peng Tian^{*a} and Zhongmin Liu^{*a}

A low-temperature strategy is developed for the synthesis of low-silica SAPO-34 with a tunable Si content and relatively uniform Si distribution in the crystals, which is hitherto difficult to achieve. It is demonstrated that a lower crystallization temperature and a silicon source with relatively low reactivity are important factors leading to successful synthesis. The crystal size of SAPO-34 could be effectively decreased to 200 nm through a seed-assisted approach. The local atom environments of low-silica samples are investigated by solid state MAS NMR, which confirms the unique existence of Si(4Al) species in the framework. The obtained low-silica SAPO-34 exhibits excellent catalytic performance in the MTO reaction and the occurrence of catalyst deactivation varies with the acid properties. Through optimizing the Si content of the samples, a long catalyst life and a high initial/maximum selectivity to ethylene plus propylene could be achieved simultaneously over SAPO-34 with a Si content of $\text{Si}/(\text{Si} + \text{Al} + \text{P}) = 0.047$. This result would be valuable for the improvement of the catalytic properties of SAPO-34 used for a commercial MTO fluidized-bed reactor. However, SAPO-34 with a very low Si content (e.g. $\text{Si}/(\text{Si} + \text{Al} + \text{P}) = 0.039$) exhibits a shortened catalyst life due to the insufficient Brønsted acid sites in spite of the high selectivity to light olefins.

Received 8th July 2016,
Accepted 2nd September 2016

DOI: 10.1039/c6cy01461e

www.rsc.org/catalysis

Introduction

Zeolites are a family of microporous crystalline materials containing uniform pores and cavities of molecular dimensions, which have been widely employed as heterogeneous acid catalysts in the petrochemical and fine chemical industries.^{1–3} In recent years, as a successful alternative route to produce light olefins from non-oil resources such as coal and natural gas, methanol-to-olefins (MTO) conversion on zeolite catalysts has aroused extensive concern and has been extensively studied.^{4–9} A variety of molecular sieves have been employed as MTO catalysts to date, and it is recognized that the silicoaluminophosphate molecular sieve SAPO-34 with a CHA topological structure shows excellent catalytic performance in the MTO process due to its moderate acid strength and ideal CHA cage.^{10–13} The diffusion of reactants and products over SAPO-34, however, would be greatly restricted once

a significant fraction of the CHA cages is occupied by polycyclic aromatics (called coke) during the MTO process, leading to the rapid deactivation of SAPO-34.^{14–16}

In consideration of the effect of the characteristics of zeolite catalysts on coking and deactivation rates, modification of the acidic properties and improvement of the diffusion properties of zeolite catalysts are two effective strategies to obtain a highly active catalyst with a prolonged lifetime.^{17–20} For SAPO-34, extensive attention has been paid to controlling the Brønsted acidity, which is closely related to Si incorporation in the framework.^{21–24} Typically, enhanced catalytic performance and coke resistance in the MTO reaction have been observed on SAPO-34 having a lower Si content, and the beneficial effects could be attributed to the lower acid density and the isolated Si(4Al) environment that exhibits moderate acid strength.^{5,25} However, intimate knowledge of the relationship between the Brønsted acid density and catalytic performance (activity/selectivity) of the low-silica SAPO-34 catalyst in the MTO reaction is still lacking. This is mainly because the synthesis of pure low-silica SAPO-34 with a low and tunable Si content ($n_{\text{Si}}/n_{(\text{Si}+\text{Al}+\text{P})} < 0.07$) still remains a challenging work, and crystal impurities tend to form together with SAPO-34 when employing a precursor gel with a low silica content.²⁶ To date, very few cases that produce low-silica SAPO-34 have been achieved, most of which involve the

^a National Engineering Laboratory for Methanol to Olefins, Dalian National Laboratory for Clean Energy, Dalian Institute of Chemical Physics, Chinese Academy of Sciences, Dalian 116023, PR China. E-mail: tianpeng@dicp.ac.cn, liuzm@dicp.ac.cn; Fax: +86 411 84379289; Tel: +86 411 84379998

^b University of Chinese Academy of Sciences, Beijing 100049, PR China

† Electronic supplementary information (ESI) available: More details of the experiment, additional XRD patterns, SEM, ¹³C MAS NMR, NH₃-TPD and porous properties of samples. See DOI: 10.1039/c6cy01461e

use of expensive tetraethylammonium hydroxide (TEAOH) as the template.^{26,27} In addition, the synthesis temperature in these procedures is generally higher than 170 °C. Therefore, it is highly desirable to develop facile strategies to synthesize SAPO-34 with a low silica content and elucidate the effect of lower Brønsted acid density on the catalytic performance in the MTO process.

Generally, crystallization temperature has a great influence on the zeolite nucleation and growth rate, which may alter the reaction process/intermediate, and lead to different crystal phases and sizes.^{28–30} Our previous work also demonstrated that low crystallization temperature could change the crystal growth habit to fabricate hierarchical AlPO-based molecular sieves without the help of surfactants.³¹ Moreover, it was also found that low-temperature crystallization may result in low efficiency for Si incorporation in the SAPO-5 product in our synthesis cases, which suggests that altering the crystallization temperature may be an effective method to tune the Si content of SAPO molecular sieves. However, hitherto no attention has been paid to modifying the SAPO compositions *via* kinetic regulation by controlling the crystallization temperature.

In the present work, a low-temperature strategy was thus rationally developed to synthesize low-silica SAPO-34 with a tunable Si content and good purity. The significance of the silicon source and crystallization temperature in the synthesis was demonstrated. The crystal size of low-silica SAPO-34 could be effectively decreased to 200 nm through a simple seed-assisted approach. Meanwhile, the MTO catalytic performances of SAPO-34s with varied low Si contents were investigated in detail. The acid densities of SAPO-34s were measured and correlated with their reaction behaviours (both lifetime and product selectivity). The advantage of nanosized low-silica SAPO-34 when it comes to the catalytic lifetime was also confirmed. This work provides not only a facile way to synthesize low-silica SAPO-34 but also useful guidance for the optimization of the SAPO-34 catalyst for the MTO reaction.

Experimental

Chemical reagents

The organic templates used in the synthesis were triethylamine (TEA, 99 wt%, Tianjin Damao Chemical Reagent Co.) and tetraethylammonium bromide (TEABr, 99 wt%, Shanghai Annaiji Chemical Reagent Co.). Pseudoboehmite (67.5 wt%, Shandong Chemical Co.), phosphoric acid (85.0 wt%, Sichuan Xianfeng Chemical Co.), and silica sol (31.0 wt%, Shenyang Chemical Co.) were used as inorganic resources. Tetraethyl orthosilicate (TEOS, 98 wt%, Tianjin Kemiou Chemical Reagent Co.) and aluminium iso-propoxide (Al(OPri)₃, 24.7 wt%, based on Al₂O₃, Sinopharm Chemical Reagent Company) were used as the organic silica source and aluminium source, respectively. All the chemicals were used without further purification.

Synthesis of low-silica SAPO-34 samples

The typical gel ratios for low-silica SAPO-34s were $x\text{TEA} : y\text{TEABr} : 0.8\text{Al}_2\text{O}_3 : 1.0\text{P}_2\text{O}_5 : z\text{SiO}_2 : 50\text{H}_2\text{O}$ and the details are shown in Table 1. Typically, the hydrothermal synthesis was performed as follows: 3.02 g of pseudoboehmite was firstly added to 17.60 g of deionized water and then 5.76 g of phosphoric acid was added to the mixture under stirring. Then, 2.43 g of silica sol was added and stirred for a certain time. After further addition of an organic amine and TEABr, the mixture was further stirred for 2–4 h and the resulting mixture was transferred into a 50 mL autoclave and heated at 120 °C for 48–96 h. After crystallization, the solid product was recovered by filtration, washed with distilled water, and dried in air. The product yield is based on the following formula: $\text{yield (\%)} = M_{\text{sample}} \times 85\% \times 100 / (M_{\text{Al}_2\text{O}_3 + \text{P}_2\text{O}_5 + \text{SiO}_2})_{\text{gel}}$, where M_{sample} , 85%, and $(M_{\text{Al}_2\text{O}_3 + \text{P}_2\text{O}_5 + \text{SiO}_2})_{\text{gel}}$ stand for the weight of the product, an estimated value of the framework compounds included in the sample, and the dry mass of inorganic oxides in the starting mixture, respectively.

Synthesis of nanosized low-silica SAPO-34s

Small amounts of ball-milled SAPO-34 were used as seeds (5, 10 and 15 wt% in relation to the sum of SiO₂, Al₂O₃, and P₂O₅ contents in the initial mixtures) for the synthesis of nanosized low-silica SAPO-34s. The preparation procedure of seeds is as follows: 10.0 g of SAPO-34 was calcined at 600 °C to remove the template. Then, it was dispersed into water and milled in a planetary ball mill (QM-3SP2, Nanjing China) at 550 rpm for 420 min. After milling, the slurry was collected and dried at 100 °C overnight. The XRD pattern of the seeds is given in Fig. S1† and it shows that the peak intensity of the milled sample decreased a lot, indicating destruction of the crystal structure. In a typical procedure, 3.02 g of pseudoboehmite was firstly added to 13.06 g of deionized water and then 5.76 g of phosphoric acid was added to the mixture under stirring. Then, 0.33 g of SAPO-34 seeds dispersed in 3.97 g of H₂O was combined with this mixture, followed by the addition of 7.85 g of TEABr and 4.92 g of TEA. The crystallization was conducted in an oven at 120 °C for 48 h. After crystallization, the product was separated from the mother liquid, washed with water, and dried at 100 °C overnight.

Synthesis of reference samples (samples H1, H2 and H3)

For comparison, conventional SAPO samples with a mixture of $a\text{TEA} : b\text{TEABr} : 0.8\text{Al}_2\text{O}_3 : 1.0\text{P}_2\text{O}_5 : c\text{SiO}_2 : 50\text{H}_2\text{O}$ were crystallized at 160 °C or 200 °C for 48 h under autogenous pressure. The synthetic procedure and material sources are the same as those used for the above samples. The detailed gel compositions for the samples are given in Table S1.†

Synthesis of reference samples templated by TEOH (samples H4 and H5)

The synthetic procedure and inorganic sources for the synthesis of sample H4 are the same as those for the above

Table 1 Synthesis conditions, crystal phases and product compositions of the SAPO molecular sieves

Sample	Gel composition ^a			<i>T</i> /°C	<i>t</i> /h	Product	Molar composition	
	<i>x</i> TEA	<i>y</i> TEABr	<i>z</i> SiO ₂				XRF ^b	XPS ^c
L1	1.5	0	0.5	120	48	SAPO-5	—	—
L2	2.0	0	0.5	120	48	No solid	—	—
L3	2.0	0.5	0.5	120	48	SAPO-34	Al _{0.517} P _{0.413} Si _{0.070}	—
L4	2.0	1.5	0.5	120	48	SAPO-34	Al _{0.495} P _{0.430} Si _{0.075}	—
L5	1.8	1.5	0.5	120	48	SAPO-34	Al _{0.510} P _{0.423} Si _{0.067}	Al _{0.450} P _{0.474} Si _{0.076}
L6	1.8	1.5	0.2	120	96	SAPO-34	Al _{0.529} P _{0.415} Si _{0.056}	—
L7	1.8	1.5	0.15	120	96	SAPO-34	Al _{0.508} P _{0.445} Si _{0.047}	—
L8	1.8	1.5	0.10	120	96	SAPO-34	Al _{0.530} P _{0.431} Si _{0.039}	—
L9	1.8	1.5	0	120	96	AlPO-18	—	—
L10	1.5	1.5	0.5	120	48	SAPO-34/18	Al _{0.491} P _{0.462} Si _{0.047}	Al _{0.450} P _{0.495} Si _{0.055}
L11 ^d	1.8	1.5	0.3	120	48	SAPO-34	Al _{0.486} P _{0.385} Si _{0.129}	—

^a The initial molar composition was as follows: *x*TEA:*y*TEABr:0.8Al₂O₃:1.0P₂O₅:*z*SiO₂:50H₂O. Si sol was used as the Si source in the gel.

^b Determined by X-ray fluorescence (XRF) analysis. ^c Determined by X-ray photoelectron spectroscopy (XPS) compositional analysis. ^d TEOS was used as the Si source.

samples except for the use of TEOAH as the template. The detailed gel composition for sample H4 is given in Table S1.†

Sample H5 was synthesized from starting gels with molar compositions of 1.0Al₂O₃:1.2P₂O₅:2.0TEAOH:0.2SiO₂:40H₂O according to the work reported by Yu *et al.*³² Typically, Al(OPrⁱ)₃ was first finely ground and mixed with a TEOAH solution and deionized water at room temperature. After it was completely dissolved, phosphoric acid was added dropwise and the mixture was further stirred for 2 h. Finally, fumed silica was slowly added. The reaction mixture was further stirred for 1 h and then was transferred into a 100 mL stainless steel autoclave. Crystallization was conducted in a conventional oven at 170 °C for 3 days under static conditions. After the crystallization, the product was centrifuged, washed with water, and dried at 100 °C overnight.

Characterization

The morphologies and the crystal sizes of the samples were observed by scanning electron microscopy (SEM, Hitachi SU8020). The particle size distribution was measured by Dynamic Light Scattering (DLS) using a Zetasizer Nano ZS (Malvern Instruments). The Nano ZS system is equipped with a 4 mW red laser (633 nm) and a detection angle of 173°. The powder XRD pattern was collected to determine the crystalline phase using a PANalytical X'Pert PRO X-ray diffractometer with Cu-Kα radiation ($\lambda = 1.54059 \text{ \AA}$) operated at 40 kV and 40 mA. The chemical compositions of the solid samples were determined using a Philips Magix-601 X-ray fluorescence (XRF) spectrometer. X-ray photoelectron spectroscopy (XPS) measurements were conducted on a Thermo ESCALAB 250Xi XPS instrument. The X-ray excitation was provided by a monochromatic Al Kα (1486.6 eV, 15 kV, 10.8 mA) source. The surface atomic concentrations were determined from the photoelectron peak areas of Si 2p, Al 2p and P 2p. Nitrogen adsorption-desorption measurements were carried out using a Micromeritics ASAP 2020 analyzer at -196 °C, after the sample was degassed at 350 °C under vacuum. The total surface

area was calculated based on the BET equation. The micropore volume, external surface area and micropore surface area were evaluated by using the *t*-plot method. The total pore volume was determined from the amount adsorbed at the relative pressure of about 0.98. The acid properties of the samples were determined by temperature-programmed desorption of ammonia (NH₃-TPD) using a Micromeritics Autochem II 2920 device. The samples (200 mg) were outgassed under a He flow at 600 °C for 60 min. Then, the samples were cooled down to 100 °C and subjected to a flow of NH₃/He for 30 min to saturate the sample with NH₃. Subsequently, a He flow was purged through the sample for 30 min to remove the weakly adsorbed NH₃ molecules. Measurement of the desorbed NH₃ was performed from 100 to 650 °C at a heating rate of 10 °C min⁻¹ under a He flow (20 mL min⁻¹). All solid state NMR experiments were performed using a Bruker Avance III 600 spectrometer equipped with a 14.1 T wide-bore magnet. The resonance frequencies in this field strength were 150.9, 156.4, 242.9 and 119.2 MHz for ¹³C, ²⁷Al, ³¹P and ²⁹Si, respectively. A 4 mm MAS probe with a spinning rate of 12 kHz was employed to acquire ³¹P, ²⁷Al and ¹³C NMR spectra. The ¹³C MAS NMR spectra were recorded with a contact time of 3 ms and a recycle delay of 4 s. The ²⁷Al MAS NMR spectra were acquired using a single pulse sequence. 200 scans were accumulated with a $\pi/8$ pulse width of 0.75 μ s and a recycle delay of 2 s. Chemical shifts were referenced to (NH₄)Al(SO₄)₂·12H₂O at -0.4 ppm. The ³¹P MAS NMR spectra were recorded using high-power proton decoupling. 32 scans were accumulated with a $\pi/4$ pulse width of 2.25 μ s and a 10 s recycle delay. Chemical shifts were referenced to 85% H₃PO₄ at 0 ppm. The ²⁹Si MAS NMR spectrum was recorded with a 7 mm MAS probe with a spinning rate of 6 kHz using high-power proton decoupling. 5000–6000 scans were accumulated with a $\pi/4$ pulse width of 2.5 μ s and a 10 s recycle delay. Chemical shifts were referenced to 4,4-dimethyl-4-silapentane sulfonate sodium salt (DSS). The ¹H MAS NMR spectra were recorded using a 4 mm MAS probe. The pulse width was 2.2 μ s for a $\pi/4$ pulse, and

32 scans were accumulated with a 4 s recycle delay. The samples were spun at 12 kHz, and chemical shifts were referenced to adamantane at 1.74 ppm.

Catalytic tests

The performance of the catalysts in the MTO reaction was tested in a quartz tubular fixed-bed reactor under atmospheric pressure. Typically, 0.3 g of calcined SAPO-34 catalysts (sieve fraction, 40–60 mesh) was loaded in the quartz reactor and activated under a nitrogen flow at 550 °C for 1 h. After cooling to the reaction temperature of 450 °C, methanol was fed by switching the carrier gas (28 mL min⁻¹) to pass through the methanol saturator containing methanol at 30 °C, corresponding to a weight hourly space velocity (WHSV) of 2.0 h⁻¹. While the MTO reaction was performed with a WHSV of 4.16 h⁻¹, methanol was fed by the carrier gas (42 mL min⁻¹) that passed through the methanol saturator containing methanol at 35 °C. The products were analyzed by an online gas chromatograph (Agilent GC 7890N) equipped with a flame ionization detector (FID) and a Plot-Q column.

The amount of generated coke in the SAPO-34 catalysts after the MTO reaction was determined by thermal analysis (TG-DTA) using a TA SDT Q600 analyzer at the temperature range of 100–900 °C with a heating rate of 10 °C min⁻¹ under an air flow of 100 mL min⁻¹.

Results and discussion

Synthesis and characterization of low-silica SAPO-34 samples

The gel compositions, synthesis conditions, and details of the obtained products are summarized in Table 1 and the corresponding XRD patterns are shown in Fig. 1 and S2.† It can be seen that no SAPO-34 product could be achieved with the use of only the organic amine TEA as the sole template (samples L1 and L2). In consideration of the better structure-directing ability of a quaternary ammonium cation than TEA, TEABr was thus introduced to the synthetic gel as a co-template. As a consequence, the pure phase of SAPO-34 was obtained under the assistance of the mixed templates (TEA/TEABr) after two days of crystallization by the low-

temperature hydrothermal route. The amount of TEABr in the synthesis gel of SAPO-34 could be modulated in a certain range, and the product yields rose obviously with the increasing TEABr content in the initial gel (33.7% solid yield for sample L3 and 48.7% for sample L4). Furthermore, the silica content in SAPO-34 could be reduced to a much lower level without the appearance of any impurity by simply lowering the silica content in the starting gel (Table 1, samples L5–L8), which is difficult to achieve through conventional methods, demonstrating the effectiveness of the present low-temperature strategy. However, AlPO₄-18 instead of AlPO₄-34 crystallized as the final product without the addition of silica in the gel, which is somewhat expected due to the fact that AlPO₄-34 generally crystallizes in a F⁻-containing system.

Fig. 1 shows the XRD patterns of the obtained SAPO-34 samples, which exhibit high crystallinity and match very well with the simulated XRD pattern of the CHA-type molecular sieve. Fig. 2 presents the SEM images of the samples, which present a typical rhombohedral morphology with an uneven surface for samples L5 and L6; however, with the further decrease of the silica concentration, the rhombohedral crystals evolve into a sheet-like morphology (samples L7 and L8). Moreover, XPS, a surface sensitive technique to analyze the surface chemical composition, was also carried out to investigate the Si distribution in the samples and the results are shown in Table 1. It was found that the surface silica content of low-silica samples is similar to the bulk elemental compositions derived from XRF analysis, suggesting a relatively uniform distribution of Si in the crystals from the core to the surface. This is different from the previously reported results for SAPO-34 samples having an obvious Si gradient (Table S2†) and is expected to be favourable for their MTO catalytic

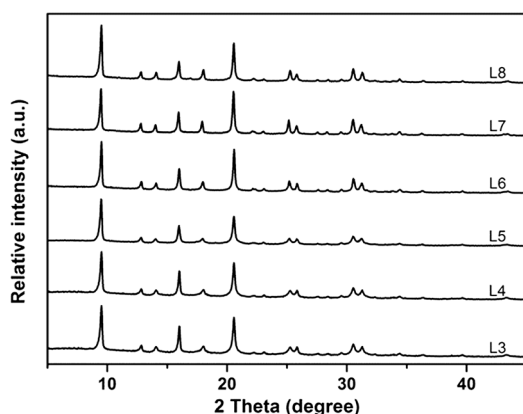


Fig. 1 XRD patterns of as-synthesized low-silica SAPO-34 samples.

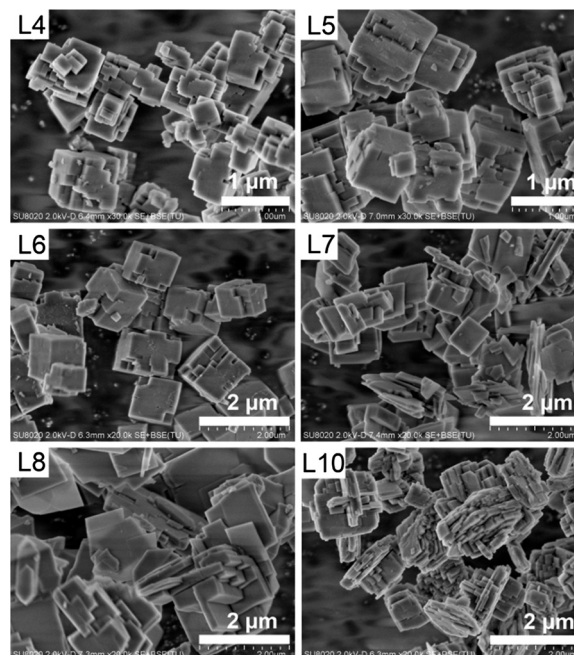


Fig. 2 SEM images of as-synthesized low-silica samples.

performance due to the decreased enrichment of acid sites on the crystal shell.^{33,34}

Generally, the hydrothermal synthesis of zeolites is a very complicated process that may be influenced by many factors. Herein, the successful synthesis of low-silica SAPO-34 is also a result of a combination of multiple factors. First, the presence of TEABr was demonstrated to be a critical factor to the synthesis, which could accelerate the crystallization process due to its better structure-directing ability. Second, the gel pH (associated with the dosage of TEA) also played an important role in the synthesis. When the molar ratio of TEA/TEABr changed from 1.8/1.5 to 1.5/1.5, the product varied from SAPO-34 (sample L5) to SAPO-34/18 (sample L10). Upon further decreasing the molar ratio of TEA/TEABr to 1.2/1.5, the product turned into a mixture of SAPO-5 and SAPO-34/18. That is, the gel pH mainly affected the product phases, as is the case in the conventional synthesis. Moreover, several control experiments were also carried out to further elucidate the parameters that are important for the formation of low-silica SAPO-34. First, the initial gel with the same composition as that of sample L5 was hydrothermally crystallized at 160 and 200 °C, respectively. Consequently, SAPO-34 with the AEI phase as an intergrowth crystallized from the gel, as evidenced by the broadening of a number of diffraction peaks and especially the emergence of a small peak at around 16.9° in the XRD reflections (samples H1 and H2, Table S1, Fig. S3†). Notably, the relative fractions of the AEI phase in the intergrowth increase with the crystallization temperature, which implies that a lower temperature affords the elimination of growth stacking faults in SAPO-34 crystals.³⁵ Moreover, the silica content of sample H2 ($\text{Al}_{0.451}\text{P}_{0.418}\text{Si}_{0.131}$) present a significant increase compared with that of sample L5 ($\text{Al}_{0.510}\text{P}_{0.423}\text{Si}_{0.067}$), and an effort to synthesize low-silica SAPO-34 at 200 °C by reducing the amount of silica in the gel resulted in the appearance of a SAPO-5 impurity (sample H3, Table S1 and Fig. S3†), confirming the pivotal role of crystallization temperature. On the other hand, the type of silica source was also demonstrated to play an essential role in the synthesis. SAPO-34 with a much higher Si content would be obtained when a monomeric silica source TEOS was used instead of silica sol (sample L11, Table 1 and Fig. S2†). This indicates that the slower depolymerization/hydrolysis rate of silica sol in the gel under low temperature is important to the final silica content of SAPO molecular sieves, which makes tuning of the silicon content possible. Therefore, employing a Si source with relatively low reactivity at low temperature is important for the present synthetic strategy.

The textural properties of selected samples were determined using N_2 adsorption–desorption measurements and the results are shown in Table 2 and Fig. S4.† All the samples exhibit the characteristic type I isotherms that give a steep increase in the curve at low relative pressures, confirming the microporosity of the samples. The large surface areas and high pore volumes confirm the good crystallinity of the samples achieved by means of the low-temperature route.

Table 2 Textural properties of the samples

Sample	Surface area ($\text{m}^2 \text{g}^{-1}$)			Pore volume ($\text{cm}^3 \text{g}^{-1}$)	
	S_{total}^a	S_{micro}^b	S_{ext}^b	V_{micro}^b	V_{meso}^c
L5	615	589	26	0.26	0.03
L7	634	626	8	0.27	0.02
L8	624	614	10	0.27	0.02
L5–10	640	588	52	0.25	0.11

^a BET surface area. ^b S_{micro} (micropore area), S_{ext} (external surface area) and V_{micro} (micropore volume) determined from the t -plot method. ^c V_{meso} (mesopore volume) = $V_{\text{total}} - V_{\text{micro}}$; V_{total} is determined from the adsorbed volume at $P/P_0 = 0.98$.

¹³C MAS NMR was employed to investigate the incorporation of amines in the products and the corresponding spectra are illustrated in Fig. S5.† For samples L3, L5 and L10 synthesized using different mole ratios of TEA/TEABr, two peaks centred at *ca.* 7 and 52.8 ppm assigned to the $-\text{CH}_3$ groups and $-\text{CH}_2-$ groups of TEA^+ , respectively, could be observed, suggesting the only inclusion of TEA^+ in the as-synthesized samples.³¹ However, the exact effect of TEA in the system is more than to adjust the pH value, for no products crystallized from the gel when other organic amines such as diethylamine were employed as a co-template with TEABr. The role of TEA in the synthesis of SAPO-34 is interesting and worthy of further research.

The chemical environments of the framework atoms of the samples were investigated by solid-state MAS NMR spectroscopy. As shown in Fig. 3(a), the ²⁹Si MAS NMR spectra of low-silica SAPO-34s present a dominant peak at -92 ppm exclusively, demonstrating the presence of Si(4Al)

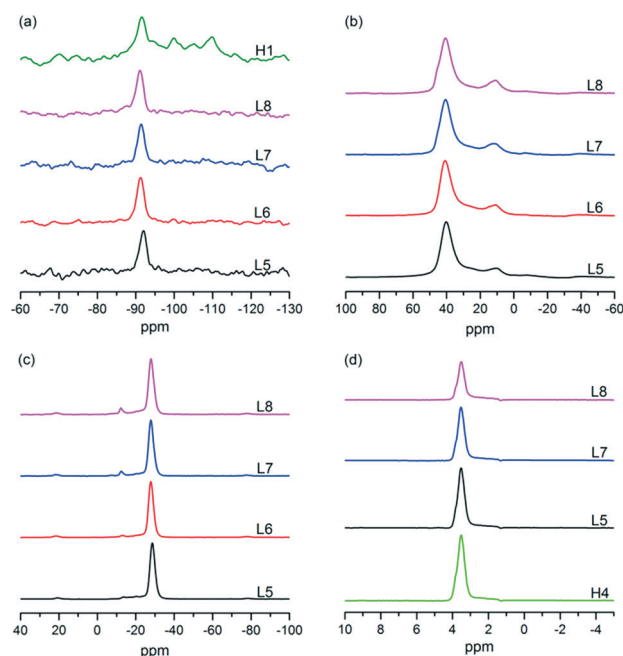


Fig. 3 ²⁹Si (a), ²⁷Al (b), ³¹P (c) and ¹H (d) MAS NMR spectra of as-synthesized low-silica SAPO samples.

species in the framework and the absence of silica islands. This is consistent with the low-silica characteristic of the samples. As a comparison, the ^{29}Si spectrum of sample H1 (SAPO-34/18 intergrowth, $\text{Al}_{0.492}\text{P}_{0.437}\text{Si}_{0.070}$) synthesized at 160 °C was also obtained and is shown in Fig. 3(a). Clearly, there are diverse silicon species in the framework of sample H1. The spectrum presents a dominant peak at -91 ppm and four overlapped peaks at around -95, -100, -105 and -110 ppm assigned to Si(1Si3Al), Si(2Si2Al), Si(3Si1Al) and Si(4Si0Al), respectively, which should result from the existence of SAPO-18 in sample H1, though it has a similar Si content to sample L5 synthesized at lower temperature. Fig. 3(b) and (c) show the ^{27}Al and ^{31}P MAS NMR spectra for low-silica SAPO-34 samples, respectively. The ^{27}Al spectra of the samples display an intense peak at 40 ppm arising from tetrahedral Al. The weak peak appearing at 10 ppm should be due to pentacoordinated Al atoms formed by interaction of water or the template with the framework Al atoms.³⁶ The ^{31}P spectra present a strong peak at -29 ppm corresponding to tetrahedral P(4Al), while the small peaks from -20 to -13 ppm could be assigned to partially hydrated P(OAl)_x(H₂O)_y species.³⁷

Since Brønsted acid sites originate from the protons on the bridged hydroxyl groups, ^1H MAS NMR was used to characterize the acidity of the calcined SAPO-34s and the obtained spectra are shown in Fig. 3(d). The strong signals at 3.6 ppm are unambiguously ascribed to bridged hydroxyl groups (Si(OH)Al), while the signals at 0–2.4 ppm with very weak intensities can be assigned to P–OH, Si–OH, and Al–OH groups on the outer crystal surface and framework defects.³⁸ After deconvolution using fitting of the Gaussian–Lorentzian function, the Brønsted acid site densities are determined to be 1.01, 0.80, 0.69 and 0.54 mmol g⁻¹ for samples H4, L5, L7 and L8, respectively (Table 3), consistent with their silicon content.

The acidic properties of the samples were further investigated by NH₃-TPD measurements and the profiles are shown in Fig. S6.† All the samples present two desorption peaks at 170–190 and 380–430 °C. The former peak corresponds to the desorption of physisorbed NH₃ and NH₃ adsorbed on lattice defects or terminal Si(OH) and Al(OH), whereas the latter one should mainly arise from the NH₃ desorption from the Brønsted acid sites (the bridged hydroxyl groups Si(OH)Al), which are the active sites in acid-catalyzed reactions. Obvi-

ously, the concentration of medium/strong acid sites of samples L5, L7 and L8 gradually drops (Table 3), in agreement with the decreasing Si content. Moreover, one can also notice a decreasing high-temperature desorption temperature following the decrease in Si content in the samples, which should result from the different concentrations of strong acid sites (diffusion limitation of NH₃ in the small apertures of SAPO-34) rather than the varied strong acid strength.

Synthesis of low-silica SAPO-34 nanocrystals under the assistance of seeds

In recent decades, the significant effect of particle size on catalyst performance has motivated researchers to develop methods of synthesizing nanoscale zeolites.^{39,40} Herein, the crystal size of low-silica SAPO-34 could be successfully decreased to approximately 200 nm through a simple seed-assisted approach. Based on the above synthetic gel, 5, 10, and 20 wt% seeds (milled SAPO-34) were introduced into the system, respectively, and the details of the set of experiments performed are listed in Table S3.† The representative XRD patterns of the samples obtained are displayed in Fig. S7.† all of which present good purity. The corresponding SEM images shown in Fig. 4 display the evolution of crystal sizes of the samples and it can be seen that all three samples had a rhombohedral morphology and the particle sizes gradually dropped with the increase in the amount of seeds. Moreover, the particle size distribution of the samples was also measured by DLS. As shown in Fig. S8.† the average particle size was reduced from 800 to 500 nm upon the addition of 5 wt% seeds. By further increasing the seed amount to 10 wt%, the average particle size dropped to 250 nm. However, a relatively small decrease in crystal size (~200 nm) was observed when the seed amount was further increased to 20 wt%.

The N₂ physisorption results of samples L5–10 are given in Table 2 and Fig. S4.† Uptake near the saturation pressure in the isotherms is observed, which can be attributed to the intercrystalline porosity formed by the agglomeration of nanocrystals. The higher values of mesopore volume and external surface of samples L5–10 are in accordance with their smaller crystal size.

Catalytic performance in the MTO reaction of low-silica SAPO-34 catalysts with different acid densities

Catalytic tests of methanol conversion were carried out in a fixed-bed reactor over SAPO-34 with different low Si contents (samples L5, L7 and L8) and the results of conversion and

Table 3 Acid densities of the samples by ^1H MAS NMR and NH₃-TPD

Sample	Si(OH)Al ^a (mmol g ⁻¹)	Medium and strong acid amount ^b (mmol g ⁻¹)
H4	1.01	0.73
L5	0.80	0.68
L7	0.69	0.52
L8	0.54	0.39

^a Calculated from ^1H MAS NMR deconvolution using the Gaussian–Lorentzian function. ^b Calculated from the high-temperature desorption peak of NH₃-TPD profiles.

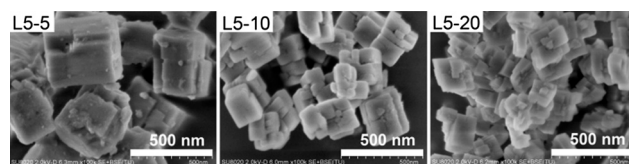


Fig. 4 SEM images of low-silica SAPO-34 nanocrystals synthesized under the assistance of different amount of seeds.

the selectivities of the products are displayed in Fig. 5. Moreover, in order to elucidate clearly the effect of acid properties on catalytic performance, SAPO-34 with a slightly higher Si content ($\text{Al}_{0.499}\text{P}_{0.418}\text{Si}_{0.083}$) and a crystal size of $\sim 1 \mu\text{m}$ was also synthesized and investigated in the MTO reaction (sample H4 in Table S1, Fig. S3 and S9†).

As shown in Fig. 5a, low-silica samples L5 ($\text{Al}_{0.510}\text{P}_{0.423}\text{Si}_{0.067}$) and L7 ($\text{Al}_{0.508}\text{P}_{0.445}\text{Si}_{0.047}$) exhibit enhanced catalytic activity compared with the reference sample H4 with a higher Si content. Specifically, the catalytic lifespan, during which $>99\%$ methanol conversion can be kept, is only 276 min for the sample H4 catalyst. Comparatively, an obviously prolonged lifetime of 393 min could be observed over low-silica samples L5 and L7, demonstrating the improved catalytic activity in methanol conversion. This indicates that the catalytic stability of SAPO-34 in the MTO reaction could be effectively increased by lowering the Si content in the catalyst. However, it is noted that sample L8 with the lowest Si content ($\text{Al}_{0.530}\text{P}_{0.431}\text{Si}_{0.039}$) exhibits an obvious decline in catalytic stability compared with samples L5 and L7. Complete methanol conversion over sample L8 can only be maintained for about 276 min, which was similar to that of the reference sample H4. However, the deactivation behaviours of the two samples differ due to their different acid densities. The low-silica sample L8 showed a slightly slower deactivation rate.

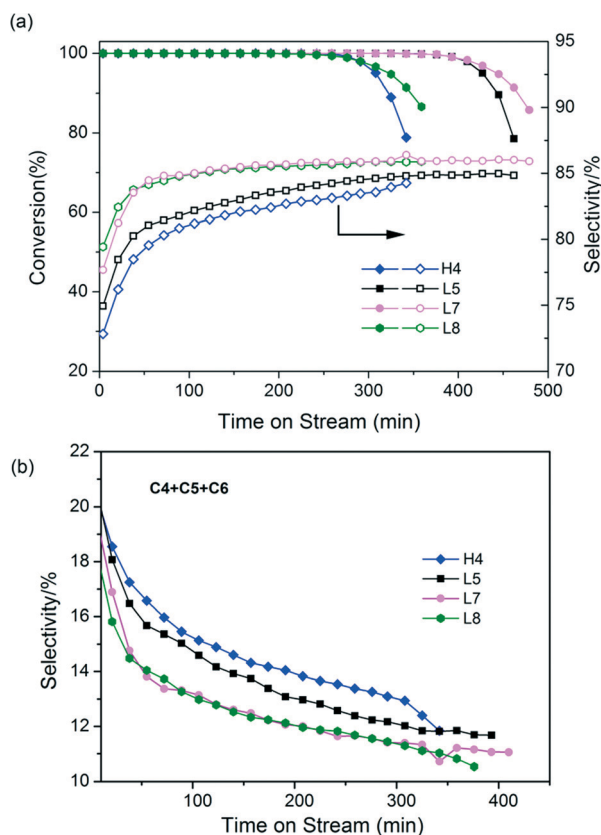


Fig. 5 Methanol conversion (a), selectivity to ethylene plus propylene (a) and C_4^+ selectivity (b) with time-on-stream over samples with different acid densities. Reaction conditions: 450°C , WHSV = 2 h^{-1} , catalyst weight = 300 mg.

Generally, the catalytic performance of acidic zeolites during the MTO process is influenced by multiple factors, such as acidity, the microporous framework structure, and crystal size.¹⁹ The formation of active intermediates and their further condensation to polycyclic aromatic hydrocarbons that cause the deactivation of the zeolite catalysts are strongly dependent on these factors. On one hand, the pore architecture of the zeolite exerts a crucial influence on the reactivity and stability in the MTO reaction.^{41,42} The intermediates generated inside the cages change with the shape and size of the cage due to spatial restrictions, which causes the cages to be blocked to different degrees. Zeolites with small pores and windows (such as SAPO-34) favor the formation of light olefins, while large pores lead to products with large dynamic diameters.⁴³ On the other hand, acidic strength and acid density are also expected to have significant effects on the formation of active intermediates and side reactions leading to coke formation, such as oligomerization, cyclization and hydrogen transfer.⁴ A higher acidic strength could decrease the energy barrier and thus increase the reaction rates.⁴⁴ However, it also accelerates the coke formation and causes a shortened catalyst lifetime. A higher concentration of Brønsted acid sites is also unfavorable for the reaction, as it would give rise to the further condensation of hydrocarbon pool compounds, accelerate coke deposits and reduce the catalyst lifetime and light olefin selectivity. Finally, zeolites with a small crystal size or hierarchical structure could effectively reduce the inherent diffusion limitations, retard coke deposition and improve the catalytic stability.⁴⁵ The effectiveness of reducing the crystal size of low-silica SAPO-34 for the MTO reaction will be also discussed later. In summary, in the MTO reaction, in addition to the pore structure, acid strength, acid density and crystallite size also determine the catalysts' MTO performances. Herein, the distinct catalytic stability among the SAPO-34 samples should mainly result from the difference in the Brønsted acid concentration as evidenced by the ^1H NMR and NH_3 -TPD results (Table 3), since the SAPO-34 catalysts tested have similar acid strengths (isolated Si(4Al) environment), crystal sizes, surface areas and pore structures. It means that there exists an optimum range of acid densities for low-silica SAPO-34 to maintain high reactivity and long-term stability in the MTO reaction.

The product distribution of the MTO reaction over the SAPO-34 catalysts is shown in Fig. 5. It can be seen that light olefins (ethylene and propylene), showing an increasing trend with time on stream, are the main products for all catalysts. Among the catalysts, the reference sample H4 displays the lowest selectivity to ethylene plus propylene (maximum of 83.3%), in accordance with it having the shortest catalytic lifetime. With the decrease of Si content in SAPO-34, the selectivity to ethylene plus propylene presents an increasing trend, and the best results are observed over samples L7 and L8, both of which give an approximate maximum value of $\sim 86\%$. In addition, both low-silica samples exhibits excellent initial selectivities to ethylene plus propylene (77.69%

and 79.43% for samples L7 and L8, respectively), which are obviously higher than those of samples L5 (74.92%) and H4 (72.82%). It is noted that a high initial selectivity to ethylene plus propylene is also important for a fluidized catalyst with SAPO-34 as the active component, considering that the fluidized-bed reactor has been adopted for the commercial MTO process.⁴ As the catalyst in the fluidized-bed reactor is always a mixture of catalysts with different coking degrees, the existence of a fresh catalyst in the reactor is inevitable and contributes to the production of light olefins. Therefore, the achievement of a high initial and maximum selectivity to ethylene plus propylene over low-silica samples L7 and L8 are very valuable and would make them good candidates for the MTO reaction, especially for sample L7 with a long catalytic lifetime. Likewise, the change in selectivity to light olefins of the catalysts should be ascribed to the different Brønsted acid concentrations. A higher amount of acid sites in sample H4 would promote the occurrence of side reactions, that is, the olefin products, which are highly active, undergo oligomerization to form heavy products and further cyclization and hydrogen transfer to form aromatic coke molecules. The formation of coke species would further cause an increasing number of successive reaction steps along the diffusion path. Correspondingly, the selectivity to alkanes (such as ethane and propane) increases, while the selectivity to light olefins drops and the catalyst lifetime is shortened. With the decrease in acid density of the catalysts, the bimolecular reactions, such as hydrogen transfer, are depressed, which results in the retainment of light olefins and the achievement of longer catalyst lifespans (this is the exact case for sample L7). Although a high selectivity to ethylene plus propylene is obtained over sample L8 having the lowest acid density, its catalyst lifetime displays an obvious decline compared with that of sample L7. It is supposed that a very low Si content of SAPO-34 would lead to insufficient acid sites, which makes the sample easier to be deactivated by the formation of heavy coke species.

The hydrogen transfer index (HTI, C_3H_8/C_3H_6)⁴⁵ was also investigated to evaluate the hydrogen transfer level of the secondary transformation of olefin products. As shown in Fig. 6, the HTI values decrease with time on stream for all samples, which is due to the formation of heavy products and the coverage of partial strong acid sites. The relatively gentle slope for samples L7 and L8 is in agreement with their lower acid density. In addition, the HTI values drop with decreasing

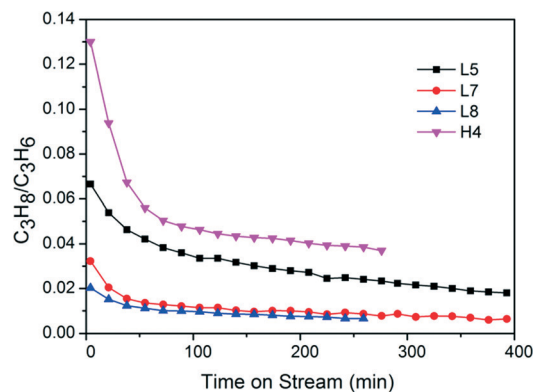


Fig. 6 Hydrogen transfer index (C_3H_8/C_3H_6) in the MTO reaction over SAPO-34 catalysts. Experimental conditions: WHSV = 2 h⁻¹, T = 450 °C, catalyst weight = 300 mg.

acid density of the catalysts, which implies the decreasing occurrence of side reactions and matches well with the high selectivity to ethylene and propylene of samples L7 and L8.

The MTO reaction over SAPO-34 has been reported to follow the aromatic-based hydrocarbon pool (HP) mechanism.^{46–48} On the other hand, our previous work demonstrated that the olefin methylation and cracking mechanism route cannot be ruled out for methanol conversion over SAPO-18 with a relatively low Brønsted acid site density.⁴⁹ Under this case, the reaction activity was very low and the formation of aromatic-based HP species was greatly restrained due to the extremely low acid concentration. Herein, given that sample L8 is active for methanol conversion and the selectivity to propylene and higher olefins does not increase in comparison with sample L5 and L7 (the olefin methylation and cracking mechanism favors the formation of propylene and C₄⁺), the aromatic-based HP mechanism should account for the catalytic performance of sample L8, which demonstrated the lowest Brønsted acid density investigated in the present work.

The crystallite size of SAPO-34 is an important factor that influences the catalytic performance, and nanosized SAPO-34 tends to exhibit a prolonged lifetime due to its shortened diffusion path.^{16,17} Herein, the MTO catalytic performances of nanoscale low-silica SAPO-34s (samples L5–10, 200–300 nm) were measured and the results are displayed in Table 4. As expected, samples L5–10 present longer catalyst lifetimes than sample L5 (~1 μm) with a high selectivity to ethylene plus propylene (maximum of 85.2%). The coke formation over the deactivated catalysts was also measured by thermal

Table 4 Catalytic performance and coke formation over SAPO-34s in the MTO reaction^a

Sample	Lifetime ^b (min)	C ₂ ^{=c} (%)	C ₃ ^{=c} (%)	C ₂ ⁼ + C ₃ ^{=c} (%)	Coke content ^d (%), g g _{cat} ⁻¹	R _{coke} ^d (g g _{cat} ⁻¹ min ⁻¹)
L5	191	51.2	33.8	85.0	23.08	0.091
L5–10	242	51.4	33.8	85.2	25.08	0.085
H5	208	48.1	35.6	83.7	—	—

^a Reaction conditions: 450 °C, WHSV = 4.16 h⁻¹, catalyst weight = 300 mg. ^b The lifetime is defined as the reaction duration with >99% methanol conversion. ^c The selectivity to C₂⁼ and C₃⁼ refers to the highest selectivity to ethylene and propylene with >99% methanol conversion. ^d Determined using a TG and DTA analyzer and measured after the MTO reaction; R_{coke} = coke content/reaction time (the reaction duration for samples L5 and L5–10 is 256 and 293 min, respectively. Both of them reach a similar methanol conversion of ~80%).

analysis and the results are given in Table 4. Considering that the deposited coke corresponds to different durations of methanol conversion for samples L5 and L5-10, we further calculated the average coking formation rate, which was defined as: coke content ($\text{g g}_{\text{cat}}^{-1}$)/reaction time (min). It could be seen that the nanosized sample has a larger capacity for coke species and a slower average coking formation rate than the microsized sample, when they reach a similar methanol conversion of $\sim 80\%$. Furthermore, low-silica SAPO-34 templated by TEOAH having a nanosheet-like morphology (~ 75 nm in thickness) was also synthesized according to the literature¹⁸ and used as a reference sample (sample H5 in Table S1 and Fig. S10,† $\text{Al}_{0.490}\text{P}_{0.441}\text{Si}_{0.069}$). The catalytic result indicates that both the lifetime and selectivity to ethylene plus propylene of the SAPO-34 catalysts obtained by the low-temperature route are comparable with or even longer than those of sample H5 synthesized with the much more expensive TEOAH (Table 4).

Conclusions

In summary, low-silica SAPO-34s with a tunable silica content and relatively uniform Si distribution in the crystals have been rationally synthesized through a facile low-temperature strategy. The adoption of low crystallization temperature and a silicon source having relatively low reactivity is revealed to be crucial to the synthesis. The composition of dual templates (TEA/TEABr) in the system could be modulated in a certain range. However, although the addition of TEA is indispensable for the synthesis, only TEA^+ is included in the products. Furthermore, the SAPO-34 crystal size could be effectively decreased to 200 nm through a simple seed-assisted approach with ball-milled SAPO-34 as seeds. The results of the MTO reaction over SAPO-34 with varying low Si contents indicate that the catalytic activity of the catalysts is strongly influenced by their Brønsted acid site density. Enhanced catalytic performance (long catalytic lifetime and high selectivity towards light olefins) could be achieved over low-silica SAPO-34 with a moderate Brønsted acid concentration and nanocrystal size. SAPO-34 having a very low Si content (e.g. $\text{Si}/(\text{Si} + \text{Al} + \text{P}) = 0.039$) would cause a reduction of the catalytic lifespan due to the insufficient Brønsted acidic sites in spite of its high selectivity to ethylene plus propylene. This facile approach for synthesizing low-silica SAPO-34 provides an alternative to other costly and complex approaches, and holds potential for the improvement of SAPO-34 catalysts in the MTO reaction. This work was supported by National Natural Science Foundation of China (21476228 and 21506207).

Notes and references

- 1 D. W. Breck, *Chemistry and Use*, Wiley, New York, 1974, vol. 636.
- 2 A. Corma, *Chem. Rev.*, 1997, 97, 2373–2420.
- 3 J. Li, A. Corma and J. Yu, *Chem. Soc. Rev.*, 2015, 44, 7112–7127.
- 4 P. Tian, Y. Wei, M. Ye and Z. Liu, *ACS Catal.*, 2015, 5, 1922–1938.
- 5 W. Dai, X. Wang, G. Wu, N. Guan, M. Hunger and L. Li, *ACS Catal.*, 2011, 1, 292–299.
- 6 U. Olsbye, S. Svelle, M. Bjørgen, P. Beato, T. V. W. Janssens, F. Joensen, S. Bordiga and K. P. Lillerud, *Angew. Chem., Int. Ed.*, 2012, 51, 5810–5831.
- 7 C. D. Chang, *Catal. Rev.: Sci. Eng.*, 1983, 25, 1–118.
- 8 D. Chen, K. Moljord and A. Holmen, *Microporous Mesoporous Mater.*, 2012, 164, 239–250.
- 9 C. Wang, Y. Wang, Y. Du, G. Yang and Z. Xie, *Catal. Sci. Technol.*, 2016, 6, 3279–3288.
- 10 J. Liang, H. Li, S. Zhao, W. Guo, R. Wang and M. Ying, *Appl. Catal.*, 1990, 64, 31–40.
- 11 M. Stöcker, *Microporous Mesoporous Mater.*, 1999, 29, 3–48.
- 12 Q. Sun, N. Wang, D. Xi, M. Yang and J. Yu, *Chem. Commun.*, 2014, 50, 6502–6505.
- 13 I. M. Dahl, H. Mostad, D. Akporiaye and R. Wendelbo, *Microporous Mesoporous Mater.*, 1999, 29, 185–190.
- 14 J. F. Haw, W. Song, D. M. Marcus and J. B. Nicholas, *Acc. Chem. Res.*, 2003, 36, 317–326.
- 15 B. Arstad and S. Kolboe, *J. Am. Chem. Soc.*, 2001, 123, 8137–8138.
- 16 D. Chen, A. Grønvold, K. Moljord and A. Holmen, *Ind. Eng. Chem. Res.*, 2007, 46, 4116–4123.
- 17 D. Barthomeuf, *Mater. Chem. Phys.*, 1987, 17, 49–71.
- 18 M. Guisnet and P. Magnoux, *Catal. Today*, 1997, 36, 477–483.
- 19 M. Guisnet, L. Costa and F. R. Ribeiro, *J. Mol. Catal. A: Chem.*, 2009, 305, 69–83.
- 20 J. Pérez-Ramírez, C. H. Christensen, K. Egeblad and J. C. Groen, *Chem. Soc. Rev.*, 2008, 37, 2530–2542.
- 21 F. D. P. Mees, P. V. Der Voort, P. Cool, L. R. M. Martens, M. J. G. Janssen, A. A. Verberckmoes, G. J. Kennedy, R. B. Hall, K. Wang and E. F. Vansant, *J. Phys. Chem. B*, 2003, 107, 3161–3167.
- 22 S. Ashtekar, S. V. V. Chilukuri and D. K. Chakrabarty, *J. Phys. Chem.*, 1994, 98, 4878–4883.
- 23 T. Álvaro-Muñoz, C. Márquez-Álvarez and E. Sastre, *Catal. Today*, 2012, 179, 27–34.
- 24 F. C. Sena, B. F. de Souza, N. C. de Almeida, J. S. Cardoso and L. D. Fernandes, *Appl. Catal., A*, 2011, 406, 59–62.
- 25 S. Wilson and P. Barger, *Microporous Mesoporous Mater.*, 1999, 29, 117–126.
- 26 A. Izadbakhsh, F. Farhadi, F. Khorasheh, S. Sahebdelfar, M. Asadi and Z. F. Yan, *Microporous Mesoporous Mater.*, 2009, 126, 1–7.
- 27 Q. Sun, N. Wang, G. Guo and J. Yu, *Chem. Commun.*, 2015, 51, 16397–16400.
- 28 V. P. Valtchev, L. Tosheva and K. N. Bozhilov, *Langmuir*, 2005, 21, 10724–10729.
- 29 E.-P. Ng, D. Chateigner, T. Bein, V. Valtchev and S. Mintova, *Science*, 2012, 335, 70–73.
- 30 S. Tanahashi, T. Moteki and T. Okubo, *Chem. Lett.*, 2012, 41, 889–891.

- 31 B. Gao, P. Tian, M. Li, M. Yang, Y. Qiao, L. Wang, S. Xu and Z. Liu, *J. Mater. Chem. A*, 2015, **3**, 7741–7749.
- 32 Q. Sun, Y. Ma, N. Wang, X. Li, D. Xi, J. Xu, F. Deng, K. B. Yoon, P. Oleynikov, O. Terasaki and J. Yu, *J. Mater. Chem. A*, 2014, **2**, 17828–17839.
- 33 M. Yang, P. Tian, C. Wang, Y. Yuan, Y. Yang, S. Xu, Y. He and Z. Liu, *Chem. Commun.*, 2014, **50**, 1845–1847.
- 34 D. Fan, P. Tian, S. Xu, D. Wang, Y. Yang, J. Li, Q. Wang, M. Yang and Z. Liu, *New J. Chem.*, 2016, **40**, 4236–4244.
- 35 W. A. Sławiński, D. S. Wragg, D. Akporiaye and H. Fjellvåg, *Microporous Mesoporous Mater.*, 2014, **195**, 311–318.
- 36 C. S. Blackwell and R. L. Patton, *J. Phys. Chem.*, 1988, **92**, 3965–3970.
- 37 Y. Watanabe, A. Koiwai, H. Takeuchi, S. A. Hyodo and S. Noda, *J. Catal.*, 1993, **143**, 430–436.
- 38 A. Buchholz, W. Wang, M. Xu, A. Arnold and M. Hunger, *Microporous Mesoporous Mater.*, 2002, **56**, 267–278.
- 39 L. Tosheva and V. P. Valtchev, *Chem. Mater.*, 2005, **17**, 2494–2513.
- 40 V. Valtchev and L. Tosheva, *Chem. Rev.*, 2013, **113**, 6734–6760.
- 41 F. Bleken, W. Skistad, K. Barbera, M. Kustova, S. Bordiga, P. Beato, K. P. Lillerud, S. Svelle and U. Olsbye, *PCCP*, 2011, **13**, 2539–2549.
- 42 J. W. Park, J. Y. Lee, K. S. Kim, S. B. Hong and G. Seo, *Appl. Catal., A*, 2008, **339**, 36–44.
- 43 W. Dai, X. Wang, G. Wu, N. Guan, M. Hunger and L. Li, *ACS Catal.*, 2011, **1**, 292–299.
- 44 F. Bleken, M. Bjørgen, L. Palumbo, S. Bordiga, S. Svelle, K.-P. Lillerud and U. Olsbye, *Top. Catal.*, 2009, **52**, 218–228.
- 45 G. Yang, Y. Wei, S. Xu, J. Chen, J. Li, Z. Liu, J. Yu and R. Xu, *J. Phys. Chem. C*, 2013, **117**, 8214–8222.
- 46 I. M. Dahl and S. Kolboe, *Catal. Lett.*, 1993, **20**, 329–336.
- 47 I. M. Dahl and S. Kolboe, *J. Catal.*, 1994, **149**, 458–464.
- 48 I. M. Dahl and S. Kolboe, *J. Catal.*, 1996, **161**, 304–309.
- 49 J. Chen, J. Li, C. Yuan, S. Xu, Y. Wei, Q. Wang, Y. Zhou, J. Wang, M. Zhang, Y. He, S. Xu and Z. Liu, *Catal. Sci. Technol.*, 2014, **4**, 3268–3277.